SCIENCE CHINA
Physics, Mechanics & Astronomy

•Article•

January 2022 Vol. 65 No. 1: 217511
https://doi.org/10.1007/s11433-021-1779-0

Unipolar electric-field-controlled nonvolatile multistate magnetic memory in FeRh/(001)PMN-PT heterostructures over a broad temperature span

Kaiming Qiao[1,2,3], Fengxia Hu[2,3,4*], Hu Zhang[1*], Ziyuan Yu[1], Xianliang Liu[1], Yuhang Liang[1], Yi Long[1], Jing Wang[2,3,5], Jirong Sun[2,3,4], Tongyun Zhao[2,6], and Baogen Shen[2,3,6*]

[1] *School of Materials Science and Engineering, University of Science and Technology Beijing, Beijing 100083, China;*
[2] *Beijing National Laboratory for Condensed Matter Physics, Institute of Physics, Chinese Academy of Sciences, Beijing 100190, China;*
[3] *School of Physical Sciences, University of Chinese Academy of Sciences, Beijing 100049, China;*
[4] *Songshan Lake Materials Laboratory, Dongguan 523808, China;*
[5] *Fujian Innovation Academy, Chinese Academy of Sciences, Fuzhou 350108, China;*
[6] *Ganjiang Innovation Academy, Chinese Academy of Sciences, Ganzhou 341000, China*

Received July 12, 2021; accepted August 27, 2021; published online November 30, 2021

Multistate magnetic memory effect in heterostructures composed of FeRh thin films with antiferromagnetic (AFM)-ferromagnetic (FM) phase transition and (001)-oriented PMN-PT substrates has been investigated. Utilizing a unipolar electric field, the nonvolatile change in magnetization was nearly doubled compared with that obtained utilizing a conventional bipolar bias. Four stable nonvolatile magnetic states were obtained over a broad temperature span, from 320 to 390 K, by adjusting the amplitude of the unipolar electric pulses, demonstrating the possibility of realizing a multistate nonvolatile magnetic memory in the FeRh/PMN-PT heterostructures. This work provides a new strategy for enhancing the magnetic response by utilizing unipolar electric fields and promotes the utilization of AFM-FM phase transition materials in multifunctional information storage and novel spintronic devices.

nonvolatile, FeRh, PMN-PT, electric-field control of magnetism

PACS number(s): 75.30.Kz, 75.50.Bb, 75.50.Ss, 75.70.Ak, 83.60.Np

Citation: K. Qiao, F. Hu, H. Zhang, Z. Yu, X. Liu, Y. Liang, Y. Long, J. Wang, J. Sun, T. Zhao, and B. Shen, Unipolar electric-field-controlled nonvolatile multistate magnetic memory in FeRh/(001)PMN-PT heterostructures over a broad temperature span, Sci. China-Phys. Mech. Astron. **65**, 217511 (2022), https://doi.org/10.1007/s11433-021-1779-0

1 Introduction

The explosive growth of data puts forward higher and stricter requirements on information storage, prompting the exploitation of random-access memories with high density, low energy consumption, and high speed. Nonvolatile magnetic memories based on the electric-field control of magnetism are one of the most promising candidates, and their high speed and low energy consumption have been demonstrated [1-5]. The key problem in realizing nonvolatile magnetic memories is to switch magnetic states in a reversible, energy-efficient, and stable manner [6]. Artificial ferromagnetic (FM)/ferroelectric (FE) multiferroic heterostructures, exhibiting magnetic and ferroelectric order simultaneously, have become a potential candidate for the realization of

*Corresponding authors (Fengxia Hu, email: fxhu@iphy.ac.cn; Hu Zhang, email: zhanghu@ustb.edu.cn; Baogen Shen, email: shenbg@iphy.ac.cn)

electric-field control of magnetism owing to their strong magnetoelectric (ME) coupling. In these systems, the magnetic state can be switched only by changing a single parameter (i.e., the applied voltage) [7-11]. However, most existing studies have focused on FM or ferrimagnetic materials combined with FE substrates (mostly $Pb(Mg_{1/3}Nb_{2/3})_{0.7}Ti_{0.3}O_3$ (PMN-PT)), such as $Co_{40}Fe_{40}B_{20}$/PMN-PT [12], Ni/PMN-PT [8], $La_{2/3}Sr_{1/3}MnO_3$/PMN-PT [13], and $CoFe_2O_4$/PMN-PT [14]. Antiferromagnetic (AFM) materials are rarely considered because of the absence of a net magnetic moment in the ground state, which renders them difficult to manipulate in a conventional manner. Actually, the stray field and susceptibility in AFM materials are so small that there is no need to consider external field disturbances in AFM memories. Therefore, it is also interesting to realize the control of the AFM order. Recently, AFM materials have been demonstrated to have a great potential as memory resistors through the manipulation of AFM anisotropic magnetoresistance (AMR) in FeRh thin films [15]. The B2-ordered FeRh alloy undergoes an AFM-FM phase transition at approximately 380 K and is in an AFM state at room temperature [16]. Indeed, in addition to temperature, the AFM-FM phase transition can be driven by other factors, such as strain [17-20], spin-polarized currents [21], and electric currents [22,23]. Among these, electric-field control of the AFM-FM phase transition through strain at the interface is one of the most energy-efficient techniques for magnetic memory applications. In particular, when a nonvolatile strain is generated through the application of electric-field pulses, the nonvolatile magnetic memory effect may be realized [6,10,24,25]. The PMN-PT single crystal is the most studied FE substrate, in which nonvolatile strain can be induced [26]. Its piezoelectric response crucially depends on the multidomain structures and the poled direction of the electric field. When poling along the (001) direction, a nonvolatile strain can be obtained in PMN-PT through 109° FE domain switching under a bipolar electric field, and its strain curves exhibit a loop-like shape [11]. However, 109° FE domain switching accounts only for ~26% of the total domain switching events in (001)-oriented PMN-PT, and the corresponding nonvolatile strain is only about 0.05% [12]. Besides, only two magnetic states have been reported utilizing this nonvolatile strain. The realization of a multistate magnetic memory would be beneficial to solve the long-standing issue of low storage density [27].

In this work, the nonvolatile compressive strain in (001)-oriented PMN-PT substrates produced via a unipolar electric field was studied over a broad temperature span and was exploited to control the AFM-FM phase transition in FeRh films. The nonvolatile manipulation of the magnetization change in FeRh films obtained through a unipolar electric field is almost double compared with that realized using a bipolar electric field. Moreover, a multistate nonvolatile control of the magnetism in a FeRh/(001)PMN-PT heterostructure was realized by adjusting the amplitude of the unipolar electric-field pulses over a broad temperature span, from 320 to 390 K. The observed multistate nonvolatile control of magnetism in this FeRh/(001)PMN-PT heterostructure is of great significance to promote the use of AFM-FM phase transition materials in multifunctional information storage and novel spintronic devices.

2 Experimental details

FeRh films were deposited onto (001)-oriented single-crystalline PMN-PT ($0.7(PbMg_{1/3}Nb_{2/3}O_3)$-$0.3PbTiO_3$) substrates (with dimensions of 5 mm (length) × 5 mm (width) × 0.5 mm (thickness)) at 1023 K. For the deposition, magnetron sputtering with a power of 30 W was used, at an argon pressure of about 0.2 Pa. The background vacuum pressure was 2×10^{-6} Pa. Subsequently, the FeRh films were annealed for 1 h *in-situ* at 1023 K and then cooled to room temperature in vacuum. The FeRh target and PMN-PT substrates were purchased. The structure and crystal orientation were characterized using a Bruker AXS D8 Discover four-circle X-ray diffraction (XRD) system with Cu-Kα radiation. The in-plane magnetization was measured using a superconducting quantum interference device (SQUID, Quantum Design) with *in-situ* electric fields applied across the thickness direction of the FeRh/PMN-PT structure via a Keithley 6517B electrometer. For the electric bias, the FeRh films served directly as the top electrode, whereas an Au layer was vapor-deposited onto the bottom of the substrate to obtain the bottom electrode. The leakage current was below 5 nA under an electric field of ±8 kV/cm. The pulse width of the electric field was less than 2 s.

3 Results and discussion

Figure 1(a) shows the XRD pattern of the FeRh/(001)PMN-PT heterostructure at room temperature. It is clear that the FeRh thin films grown onto the (001)-oriented PMN-PT substrates are well oriented along the [011] direction, which is consistent with our previous study [19]. To confirm the AFM-FM phase transition properties of the FeRh thin films, the temperature dependent magnetization (*M*-*T*) curves were measured using magnetic fields of 0.5 and 5 T along the in-plane [110] direction. The results are shown in Figure 1(b). A consecutive two-step phase transition occurs in the FeRh/(001)PMN-PT heterostructure, which has been demonstrated to be related to the multi-FE domains in PMN-PT substrates in our previous study [19]. As for the bulk, an external magnetic field can shift the phase transition to a lower temperature also for the FeRh films. With the assistance of a

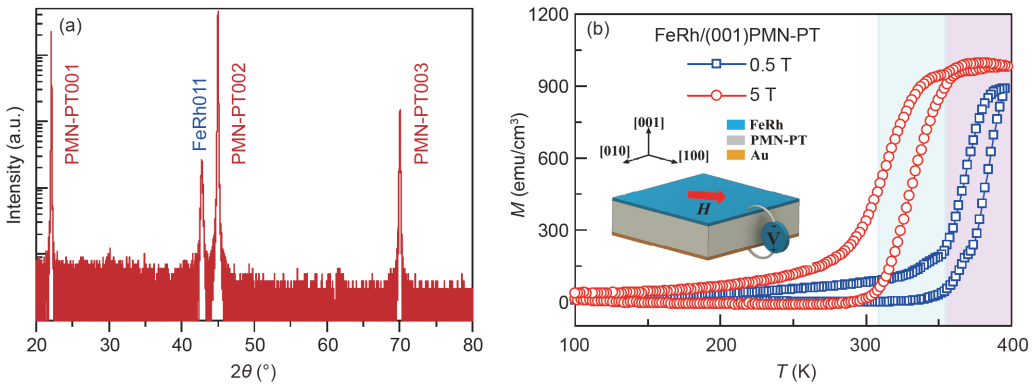

Figure 1 (Color online) (a) XRD patterns of the FeRh/(001)PMN-PT heterostructure at room temperature. (b) Temperature dependent magnetization (*M-T*) curves of the FeRh/(001)PMN-PT heterostructure measured at magnetic fields of 0.5 and 5 T. The temperature ranges across which the phase transition occurs on heating are marked by shadow areas. The inset shows a sketch of the FeRh/(001)PMN-PT heterostructure with the *in-situ* applied electric field, where *H* and *V* represent the applied magnetic field and electric field, respectively.

magnetic field, the phase transition temperature span can be broadened to be 320-400 K, as marked by the shadowed area in Figure 1(b).

Figure 2(a) shows the sketch of the FE domain evolution in a (001)-oriented PMN-PT single crystal with vertical electric field poling; a large compressive strain along the in-plane [110] direction is generated in the substrate and exerted on the FeRh film. To study the strain-mediated ME effect in the FeRh/(001)PMN-PT heterostructure, the electric field tuning of the magnetization (*M-E* curves) under bipolar sweeping of the electric field (0→+8→0→−8→0 kV/cm) was measured in the phase transition temperature span of 320-390 K, with the magnetic field along the in-plane [110] direction and the electric field along the out-of-plane [001] direction (see the sketch in the inset of Figure 1(b)). Although different magnetic fields were adopted at different temperatures, similar phenomena were observed over the whole temperature span. A representative temperature of 320 K was chosen to illustrate the manipulation of magnetism with the assistant of a 5 T magnetic field. To eliminate the influence of the diamagnetic signal of the substrate and facilitate comparison, the change in magnetization (ΔM) was used for all the results. Figure 2(b) shows two consecutive cycles of the ΔM-E curves under a bipolar electric field of ±8 kV/cm (the arrows indicate the sweep direction). The ΔM-E response exhibited an asymmetric butterfly-like curve with a coercive field of 1.8 kV/cm, which is similar to that of the strain-mediated FM/FE heterostructure reported in a previous study [25]. Repeated measurements demonstrated consistent results (see the first and second cycles in Figure 2(b)). Actually, this type of asymmetric butterfly-like *M-E* curve can be separated into butterfly-like (Figure S1(b)) and loop-like (Figure S1(c)) parts; the asymmetric response is related to FE domain switching and the R-M_A phase transition [25,28] stated above. In the initial state at 0 kV/cm, the rhombohedral (R) phase and monoclinic (M_A) phase coexist because of the polarization of the (001)-oriented PMN-PT substrates. Under the bipolar sweeping of the electric field from 0 to +8 kV/cm in Figure 2(b), the M_A phase is first totally transformed into R phase before the electric field reaches E_C = +1.8 kV/cm. During this process, the compressive strain is released so that the magnetization increases. As the electric field increases further, FE domain switching (②-③) and the R-M_A phase transition (③-④) occur, in which a large compressive strain is generated and results in a decrease in the magnetization for $E > E_C$. Under the bipolar sweeping of the electric field from +8 to 0 kV/cm, the M_A phase is partially converted into the R phase; thus, the magnetization increases. Similar to the case of the positive electric field, under 0→−8 kV/cm, the M_A-R phase transition continues, and the R phase is totally recovered when the electric field reaches the coercive electric field of −1.8 kV/cm. Thus, the magnetization increases further as the electric field increases from 0 to −1.8 kV/cm. As the electric field increases further, FE domain switching (③-②) and R-M_A phase transition (②-①) occur, leading to a decrease in the magnetization. Throughout the electric-field cycle (0→+8→0→−8→0 kV/cm), the 109° FE domain switching generates loop-like *M-E* curves (Figure S1(c)), whereas the 71°/180° FE domain switching and R-M_A phase transition generate a butterfly-like *M-E* curves (Figure S1(b)). Therefore, an asymmetric butterfly-like *M-E* curve occurs under the bipolar electric field in Figure 2(b). In previous studies, only the loop-like part of the *M-E* curve originating from the 109° FE domain switching in (001)-PMN-PT single crystals was used to obtain the nonvolatile control of magnetization in FM materials, whereas the butterfly-like part was considered to be volatile. However, the 109° FE domain switching, which generates the nonvolatile strain, accounts only for about 26% of all the domain switching events [12]. Besides, it has been demonstrated that 109° FE domain switching does not exist in all (001)-PMN-PT samples. The defects or their configurations in the crystals also play an important role in the occurrence of 109° FE domain switching. The butterfly-like part is more common in

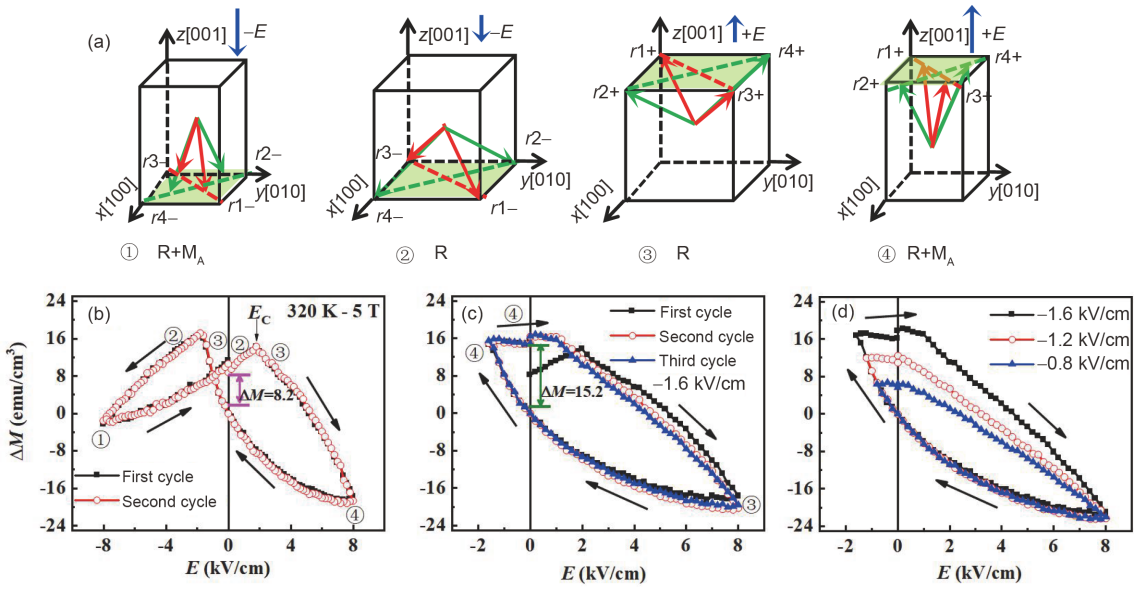

Figure 2 (Color online) (a) Sketch of the FE domain evolution in a PMN-PT single crystal during poling along the [001] direction. The direction and magnitude of the electric field are marked by the direction and length of the blue arrows, respectively. Electric-field dependent magnetization (ΔM-E) curves under (b) bipolar sweeping of the electric field to ±8 kV/cm, (c) unipolar sweeping of the electric field to −1.6 and +8 kV/cm, and (d) unipolar sweeping of different electric fields to −1.6/+8 kV/cm,−1.2/+8 kV/cm, and −0.8/+8 kV/cm, with the electric field applied along the out-of-plane [001] direction and the magnetic field along the in-plane [110] direction in the FeRh/(001)PMN-PT heterostructure. All the relevant states labeled by the circled numbers in (a) are correspondingly marked in the ΔM-E curves in (b) and (c).

(001)-PMN-PT single crystals, but is believed to be volatile. All the above aspects are detrimental for applications based on the nonvolatile strain in FM/FE heterostructures. Herein, we propose to utilize the butterfly-like part of the strain in (001) PMN-PT single crystals to induce a nonvolatile strain via a unipolar electric field. To confirm the generation of the nonvolatile strain, the ΔM-E curves under unipolar sweeping of the electric field (0→+8→0→−1.6→0 kV/cm) were measured over the whole phase transition temperature span. The ΔM-E curves resulting from three consecutive cycles at a temperature of 320 K and a magnetic field of 5 T are shown in Figure 2(c). Under the first cycle of unipolar sweeping of the electric field from 0 to +8 kV/cm in Figure 2(c), the R phase is first totally recovered when the electric field reaches the coercive electric field of +1.8 kV/cm, and the magnetization increases. As the electric field increases further, FE domain switching and the R-M_A phase transition occur and the magnetization decreases because of the induced compressive strain, which is the same as that in the bipolar process. Under unipolar sweeping of the electric field from +8 to 0 and then to −1.6 kV/cm, the M_A-R phase transition occurs, and the compressive strain decreases gradually, leading to an increase in the magnetization. However, it cannot be totally recovered because the unipolar electric field of −1.6 kV/cm is smaller than the coercive field. Under unipolar sweeping of the electric field from −1.6 to 0 kV/cm, the FE polarization remains unchanged. In the next cycle, from 0 to +8 kV/cm, FE domain switching cannot take place, and the increase in the magnetization disappears as the electric field goes from 0 to +1.8 kV/cm. The magnetization also remains almost unchanged when the electric field is smaller than the coercive field. When the electric field is larger than the coercive field, both the R-M_A phase transition (③-④ in Figure 2(b)) and the M_A-R phase transition (④-③ in Figure 2(b)) occur after removing the electric field. However, it cannot totally recover at zero field; thus, the polarization in this case is different from that obtained after removing the unipolar electric field of −1.6 kV/cm. Therefore, the ΔM-E curves in Figure 2(c) form. During this process, a nonvolatile strain is generated between two residual states at zero electric field arising from the R-M_A phase transition. Therefore, a stable and reversible magnetization change ΔM between +0 and −0 kV/cm was obtained, as can be seen clearly from Figure 2(c). The value of this reversible magnetization change reaches ΔM = 15.2 emu/cm^3, which is almost twice as large as that obtained under the bipolar electric field of ±8 kV/cm (ΔM = 8.2 emu/cm^3) shown in Figure 2(b). This enhancement in the magnetization change ΔM is crucial for magnetic memory applications considering the convenience of signal detection and high-resolution requirements. Repeated measurements demonstrate that the ΔM-E curves exhibit strong consistency (see the red and blue curves in Figure 2(c)) after the first cycle. More importantly, a multistate control of the magnetism in the FeRh/(001)PMN-PT heterostructure can be realized by adjusting the amplitude of the unipolar electric field. Figure 2(d) shows the ΔM-E curves under three different unipolar electric fields (+8/−1.6, +8/−1.2, +8/−0.8 kV/cm) at 320 K and 5 T. ΔM (−0) in the FeRh films decreases as the amplitude of the unipolar electric field decreases, whereas ΔM (+0) in the three cases is almost the

same. In particular, the ΔM values after removing the negative unipolar electric fields of −1.6, −1.2, and −0.8 kV/cm remain almost unchanged, which is beneficial for nonvolatile magnetic memories. On increasing the temperature, the electric-field tuning of the magnetization follows the same law, except for a reduction in the magnetic field. Above 370 K, the assistant magnetic field is no longer required. This indicates the potential application of FeRh thin films in magnetic memories over a broad temperature span.

Based on the electric-field control of magnetism in the FeRh/(001)PMN-PT heterostructure, nonvolatile switching of the magnetization can be realized via unipolar electric-field pulses. The multistate switching of the magnetization in FeRh thin films was investigated by applying selective unipolar electric-field pulses of −1.6, −1.2, and −0.8 kV/cm over the whole temperature span of the AFM-FM phase transition. The results at 350 K-2 T, 320 K-5 T, 390 K-0.01 T are shown in Figure 3(a)-(c). It can be seen clearly that the magnetic states can be well controlled by adjusting the electric-field pulses (−1.6, −1.2, and −0.8 kV/cm) to fully or partially transform the M_A phase into the R phase. Consequently, four stable nonvolatile magnetic states are obtained, which can be reproduced after many repeated cycles. The results at different temperatures (Figure 3(a)-(c)) follow the same law, demonstrating a multistate nonvolatile magnetic memory based on the FeRh/PMN-PT heterostructure over a broad temperature span. However, the magnetization exhibits a pronounced increase after applying the positive electric-field pulse, and this magnetization increase is different at various temperatures. This behavior may be related to the phase transition dynamics of the FeRh alloy [29,30]. The AFM-FM phase transition in the FeRh alloy can be induced by both a magnetic field and stress/strain. A compressive (tensile) strain favors the FM (AFM) phase and increases (decreases) the magnetization. As mentioned before, when an electric field is applied vertically to the (001)-PMN-PT single crystal, a compressive strain is induced along the in-plane [110] direction. When the electric field is removed, the compressive strain is partially reduced, leading to an increase in the magnetization. As a result of the dynamics of the strain-induced phase transition in FeRh alloys, the magnetization varies notably with time. When a negative electric field is removed, the induced strain remains almost unchanged. Therefore, the magnetization remains almost unchanged while applying a negative electric-field pulse. Considering the application requirements, the retention properties of the ΔM states were also investigated, and the corresponding representative results at 350 K and 2 T are

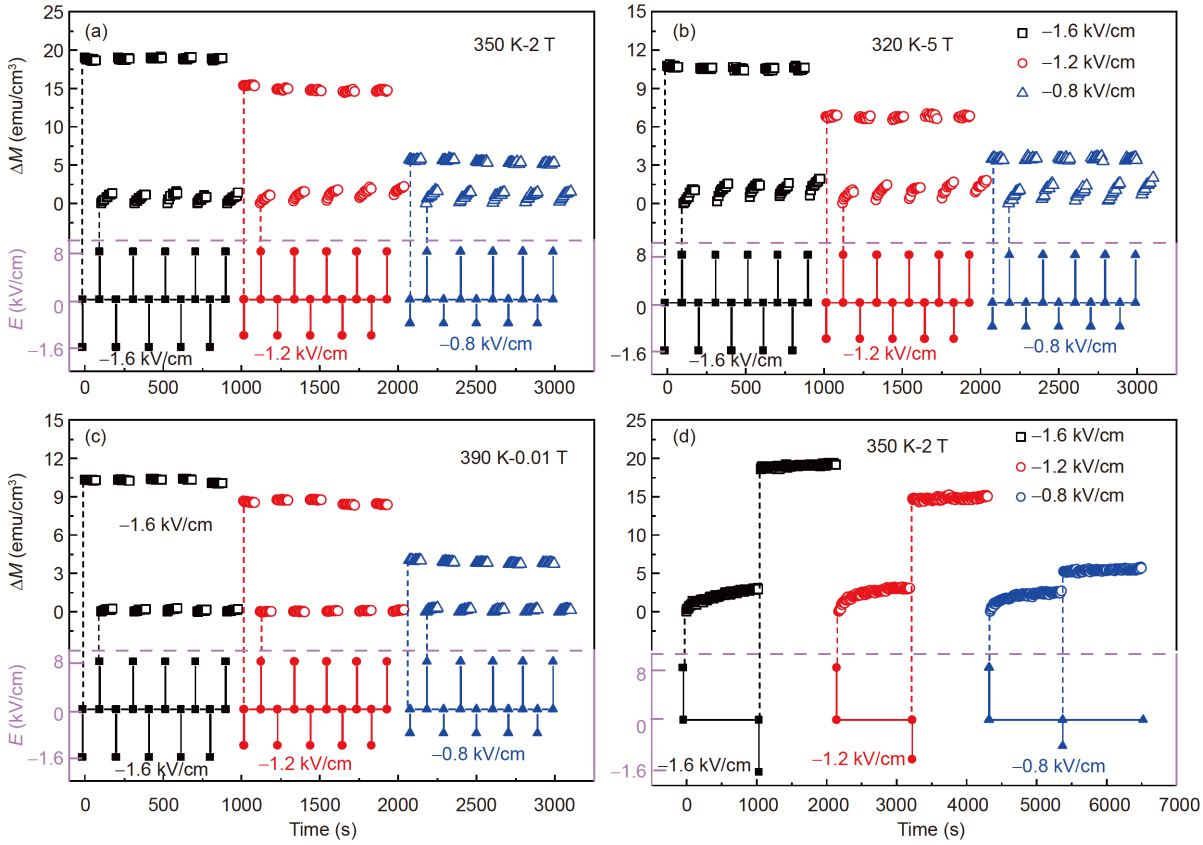

Figure 3 (Color online) Repeatable multistate switching of the magnetization obtained through the application of selective unipolar electric-field pulses of −1.6, −1.2, and −0.8 kV/cm at (a) 350 K, 2 T, (b) 320 K, 5 T, and (c) 390 K, 0.01 T. (d) Retention of the magnetic states of the FeRh films after positive (+8 kV/cm) and selective negative electric-field pulses (−1.6, −1.2, and −0.8 kV/cm) at 350 K, 2 T. In the lower panel of every image, the exploded diagram of the electric-field evolution corresponding to the above magnetic measurement process is given.

shown in Figure 3(d). As can be seen from this figure, the magnetization was measured continuously for more than 1000 s after applying the electric-field pulses. The magnetization remains almost unchanged while applying the negative unipolar electric-field pulses, whereas a noticeable relaxation occurs while applying the positive electric-field pulses. After thousands of seconds, the magnetization stabilizes gradually and is characterized by four well-defined magnetic states. These results demonstrate that the electric-field-controlled magnetization is stable, distinct, tunable, and nonvolatile, further confirming the possibility of obtaining a multistate nonvolatile magnetic memory based on the FeRh/PMN-PT heterostructure over a broad temperature span.

4 Conclusion

In conclusion, by utilizing unipolar electric fields, the nonvolatile change in magnetization obtained in FeRh/(001) PMN-PT heterostructure was found to be nearly doubled compared with that induced by utilizing bipolar electric fields. Moreover, four stable, nonvolatile magnetic states were realized over a broad temperature span, from 320 to 390 K, by adjusting the amplitude of the unipolar electric-field pulses. These results demonstrate the realization of a multistate nonvolatile magnetic memory based on the FeRh/(001)PMN-PT heterostructures over a broad temperature span. This work is important for the realization of low power consumption and high speed magnetic random-access memory utilizing these AFM-FM phase transition materials.

This work was supported by the National Key Research and Development Program of China (Grant Nos. 2020YFA0711502, 2019YFA0704900, 2018YFA0305704, and 2017YFB0702704), National Natural Science Foundation of China (Grant Nos. 52088101, U1832219, 51771223, 51971240, and 51671022), China Postdoctoral Science Foundation (Grant No. 2021M690346), Fundamental Research Funds for the Central Universities and the Youth Teacher International Exchange & Growth Program (Grant Nos. FRF-GF-20-08B, and QNXM20210014), State Key Lab of Advanced Metals and Materials (Grant No. 2019-Z11), and Key Program and Strategic Priority Research Program (B) of the Chinese Academy of Sciences (Grant No. XDB33030200).

Supporting Information

The supporting information is available online at http://phys.scichina.com and https://link.springer.com. The supporting materials are published as submitted, without typesetting or editing. The responsibility for scientific accuracy and content remains entirely with the authors.

1 S. H. Baek, H. W. Jang, C. M. Folkman, Y. L. Li, B. Winchester, J. X. Zhang, Q. He, Y. H. Chu, C. T. Nelson, M. S. Rzchowski, X. Q. Pan, R. Ramesh, L. Q. Chen, and C. B. Eom, Nat. Mater. **9**, 309 (2010).
2 S. M. Wu, S. A. Cybart, P. Yu, M. D. Rossell, J. X. Zhang, R. Ramesh, R. C. Dynes, Nat. Mater. **9**, 756 (2010).
3 J. Ma, J. Hu, Z. Li, and C. W. Nan, Adv. Mater. **23**, 1062 (2011).
4 W. Eerenstein, N. D. Mathur, and J. F. Scott, Nature **442**, 759 (2006).
5 M. Liu, O. Obi, J. Lou, Y. Chen, Z. Cai, S. Stoute, M. Espanol, M. Lew, X. Situ, K. S. Ziemer, V. G. Harris, and N. X. Sun, Adv. Funct. Mater. **19**, 1826 (2009).
6 M. Liu, T. Nan, J. M. Hu, S. S. Zhao, Z. Zhou, C. Y. Wang, Z. D. Jiang, W. Ren, Z. G. Ye, L. Q. Chen, and N. X. Sun, NPG Asia Mater. **8**, e316 (2016).
7 Y. Ba, Y. Liu, P. Li, L. Wu, J. Unguris, D. T. Pierce, D. Yang, C. Feng, Y. Zhang, H. Wu, D. Li, Y. Chang, J. Zhang, X. Han, J. Cai, C. W. Nan, and Y. Zhao, Adv. Funct. Mater. **28**, 1706448 (2018).
8 T. Wu, A. Bur, P. Zhao, K. P. Mohanchandra, K. Wong, K. L. Wang, C. S. Lynch, and G. P. Carman, Appl. Phys. Lett. **98**, 012504 (2011), arXiv: 1104.5372.
9 M. Liu, J. Hoffman, J. Wang, J. Zhang, B. Nelson-Cheeseman, and A. Bhattacharya, Sci. Rep. **3**, 1876 (2013), arXiv: 1307.0838.
10 M. Liu, B. M. Howe, L. Grazulis, K. Mahalingam, T. Nan, N. X. Sun, and G. J. Brown, Adv. Mater. **25**, 4886 (2013).
11 Y. Liu, Y. Zhao, P. Li, S. Zhang, D. Li, H. Wu, A. Chen, Y. Xu, X. F. Han, S. Li, D. Lin, and H. Luo, ACS Appl. Mater. Interfaces **8**, 3784 (2016).
12 S. Zhang, Y. G. Zhao, P. S. Li, J. J. Yang, S. Rizwan, J. X. Zhang, J. Seidel, T. L. Qu, Y. J. Yang, Z. L. Luo, Q. He, T. Zou, Q. P. Chen, J. W. Wang, L. F. Yang, Y. Sun, Y. Z. Wu, X. Xiao, X. F. Jin, J. Huang, C. Gao, X. F. Han, and R. Ramesh, Phys. Rev. Lett. **108**, 137203 (2012).
13 Y. Yang, M. M. Yang, Z. L. Luo, H. Huang, H. Wang, J. Bao, C. Hu, G. Pan, Y. Yao, Y. Liu, X. G. Li, S. Zhang, Y. G. Zhao, and C. Gao, Appl. Phys. Lett. **100**, 043506 (2012).
14 C. H. Chang, P. Yu, and C. S. Yang, Appl. Phys. Lett. **94**, 051114 (2009).
15 X. Marti, I. Fina, C. Frontera, J. Liu, P. Wadley, Q. He, R. J. Paull, J. D. Clarkson, J. Kudrnovský, I. Turek, J. Kuneš, D. Yi, J. H. Chu, C. T. Nelson, L. You, E. Arenholz, S. Salahuddin, J. Fontcuberta, T. Jungwirth, and R. Ramesh, Nat. Mater. **13**, 367 (2014), arXiv: 1503.05604.
16 S. A. Nikitin, G. Myalikgulyev, A. M. Tishin, M. P. Annaorazov, K. A. Asatryan, and A. L. Tyurin, Phys. Lett. A **148**, 363 (1990).
17 R. O. Cherifi, V. Ivanovskaya, L. C. Phillips, A. Zobelli, I. C. Infante, E. Jacquet, V. Garcia, S. Fusil, P. R. Briddon, N. Guiblin, A. Mougin, A. A. Ünal, F. Kronast, S. Valencia, B. Dkhil, A. Barthélémy, and M. Bibes, Nat. Mater. **13**, 345 (2014).
18 K. Qiao, F. Hu, Y. Liu, J. Li, H. Kuang, H. Zhang, W. Liang, J. Wang, J. Sun, and B. Shen, Nano Energy **59**, 285 (2019).
19 K. Qiao, J. Wang, F. Hu, J. Li, C. Zhang, Y. Liu, Z. Yu, Y. Gao, J. Su, F. Shen, H. Zhou, X. Bai, J. Wang, V. Franco, J. Sun, and B. Shen, Acta Mater. **191**, 51 (2020).
20 J. Chen, J. Ma, Y. Zhang, S. Bao, L. Wu, C. Liu, and C. W. Nan, J. Appl. Phys. **121**, 194101 (2017).
21 T. Naito, I. Suzuki, M. Itoh, and T. Taniyama, J. Appl. Phys. **109**, 07C911 (2011).
22 T. Moriyama, N. Matsuzaki, K. J. Kim, I. Suzuki, T. Taniyama, and T. Ono, Appl. Phys. Lett. **107**, 122403 (2015), arXiv: 1507.06138.
23 M. Jiang, X. Z. Chen, X. J. Zhou, B. Cui, Y. N. Yan, H. Q. Wu, F. Pan, and C. Song, Appl. Phys. Lett. **108**, 202404 (2016).
24 B. Peng, C. Zhang, Y. Yan, and M. Liu, Phys. Rev. Appl. **7**, 044015 (2017).
25 L. Yang, Y. Zhao, S. Zhang, P. Li, Y. Gao, Y. Yang, H. Huang, P. Miao, Y. Liu, A. Chen, C. W. Nan, and C. Gao, Sci. Rep. **4**, 4591 (2014).
26 T. Wu, P. Zhao, M. Bao, A. Bur, J. L. Hockel, K. Wong, K. P. Mohanchandra, C. S. Lynch, and G. P. Carman, J. Appl. Phys. **109**, 124101 (2011).
27 Y. Wei, C. Gao, Z. Chen, S. Xi, W. Shao, P. Zhang, G. Chen, and J. Li, Sci. Rep. **6**, 30002 (2016).
28 H. Cao, F. Bai, N. Wang, J. Li, D. Viehland, G. Xu, and G. Shirane, Phys. Rev. B **72**, 064104 (2005), arXiv: cond-mat/0504037.
29 J. Leib, J. E. Snyder, T. A. Lograsso, D. Schlagel, and D. C. Jiles, J. Appl. Phys. **95**, 6915 (2004).
30 H. W. Zhang, F. Wang, T. Y. Zhao, S. Y. Zhang, J. R. Sun, and B. G. Shen, Phys. Rev. B **70**, 212402 (2004).